Case Studies in Thermal Engineering 26 (2021) 101102

Contents lists available at ScienceDirect

Case Studies in Thermal Engineering

journal homepage: www.elsevier.com/locate/csite

Bio-convective Darcy-Forchheimer periodically accelerated flow of non-Newtonian nanofluid with Cattaneo–Christov and Prandtl effective approach

Yi-Xia Li [a], Kamel Al-Khaled [b], Sami Ullah Khan [c], Tian-Chuan Sun [d,*], M. Ijaz Khan [e,**], M.Y. Malik [f]

[a] College of Mathematics and Finance, Xiangnan University, Chenzhou, 423000, PR China
[b] Department of Mathematics & Statistics, Jordan University of Science and Technology, P.O. Box 3030, Irbid, 22110, Jordan
[c] Department of Mathematics, COMSATS University Islamabad, Sahiwal, 57000, Pakistan
[d] Qiuzhen College, Huzhou University, Huzhou, 313000, PR China
[e] Department of Mathematics and Statistics, Riphah International University I-14, Islamabad, 44000, Pakistan
[f] Department of Mathematics, College of Sciences, King Khalid University, Abha, 61413, Saudi Arabia

ARTICLE INFO

Keywords:
Casson nanoliquid
Variable thermal conductivity
Cattaneo–christov theory
Gyrotactic microorganisms
Activation energy

ABSTRACT

The thermal applications of nanofluids significantly improved the heat and mass transfer pattern which convey necessary role in many engineering and industrial zones. The consideration of nanofluids contributes many dynamic applications in the solar energy and thermal engineering problems. Moreover, the stability of nanofluids is enhanced perfectively with motile microorganisms which have applications in petroleum sciences, biofuels, bio-engineering, bio-medical, enzymes etc. This research determines the applications of bio-convection in Casson nanoliquid flow subject to the variable thermal conductivity and inertial forces. The Cattaneo–Christov relations are treated to modify the heat and concentration equations. The accelerated surface with sinusoidal type velocity induced the flow. The flow problem is formulated in terms of partial differential equations. The homotopic scheme is followed in order to suggest the analytical relations. After highlighting the convergence region, the graphical simulations with help of MATHEMAITCA are performed. The physical output is addressed in view of all flow parameters. The 3-D behavior of velocity, temperature, concentration and microorganisms is also addressed.

1. Introduction

Owing to the enhanced thermophysical characteristics of nanoparticles, scientists have engaged their special attention on this topic in recent times. With impressive thermal consequences, the nano-materials reflects significances in various phenomenon like cooling of devices, thermal transport systems, energy production, bio-medical sciences, chemical processes, fission and fusion reactions, nuclear technology etc. The idea of nanofluid brings a development in the era of thermal engineering and various industrial and engineering processes. With enhanced thermal mechanism, the nanofluid reflects pioneer attention of many scientists in this century. The nanofluid contains ultra high thermal features which make the versatile. The applications of nanofluid are comprehensively noted in the solar

* Corresponding author. Qiuzhen College, Huzhou University, Huzhou, 313000, PR China.
** Corresponding author. Department of Mathematics, College of Sciences, King Khalid University, Abha, 61413, Saudi Arabia.
E-mail addresses: suntch@zjhu.edu.cn (T.-C. Sun), mikhan@math.qau.edu.pk (M. Ijaz Khan).

https://doi.org/10.1016/j.csite.2021.101102
Received 21 April 2021; Received in revised form 7 May 2021; Accepted 22 May 2021
Available online 30 May 2021

systems, thermal transport processes, nuclear reactors, cooling of devices, technological involution, bio-engineering, medical sciences etc. The size of such particles is usually noted less than 10 nm. In health sciences, the nanoparticles are recently used to damage the cancerous cells and diagnosis of some diseases. Choi [1] reported the fundamental thermal prospective of nano-materials on the basis of experimental observations. The thermophoretic and Brownian factors in nanofluid were pointed out by Buongiorno [2]. Hashim [3] notified the thermal incorporation of GO-nanoparticles adjusted to the thin needle. Turkyilmazoglu [4] addressed the hydrodynamic analysis nanofluids in view of stability mechanism. The entropy generation pattern regarding the Carreau nanofluid was reported in the investigation of Khan et al. [5]. Hajizadeh et al. [6] utilized the nanofluids between two plates with vertical pattern to address the nanofluid properties. Khan et al. [7] intended the heat transfer observations in micropolar nanofluid flow. Majeed et al. [8] visualized the thermal improvement in babe liquid by using the Fe_3O_4 nanoparticles along with dipole applications. Ashraf et al. [9] presented insight thermal performances by using the nanoparticles in blood flow following the peristaltic transport. Khan et al. [9] enrolled the dominant contribution of activation energy in Carreau non-Newtonian nanoliquid. Khan and Alzahrani [10] examined the activation energy flow of nanofluid in presence of mixed convection features. The slip flow in presence of magneto-nanoparticles with radio-active applications was worked out by Bhatti et al. [11]. Nisar et al. [12] examined the thermal important of Eyring-Powell nanofluid subject to the radiation enrollment. Bhatti [13] inspected the thermal prospective of gold nanoparticles and claimed the applications in the nanomedicine. Elkhair et al. [14] addressed the hybrid nanofluid characteristics for peristaltic transport with magnetic force features. The thermal assessment of magnetic-nanoparticles with exponential temperature-dependent viscosity was examined by Shahid et al. [15]. Bhatti et al. [16] visualized the blood flow of nanofluids with microorganism. The bioconvection pattern in based on the impulsive transport of macroscopic fluids and observed as another devoted research area in bio-engineering and biotechnology. The pattern of bioconvection is accessed as multifaceted interaction of microorganisms at various physical scales. The locomotion of self objected microorganisms induced the bioconvection pattern. The microorganism pattern is considered as meso-scale phenomenon. The motion of nanoparticles is free of microorganisms swimming and thus, the interaction between nano-materials and bioconvection leads to the more fascinating microfluidic applications. Kuznetsov [17,18] pointed out the prime features and significant prospective of bioconvection. Uddin et al. [19] performed the computational analysis determining the bio-convection aspects of nano-materials with slip mechanism. Alwatban et al. [20] addressed numerically the aspects of Eyring-Powell nanofluid with microorganisms and activation energy relations. Khan et al. [21] claimed the bio-convective transport of thixo-tropic nanofluid with mixed convection phenomenon. The development of bio-convective pattern in optimized flow of nanoparticles with disk configuration was inspected by Khan et al. [22]. Song et al. [23] addressed the nanofluid thermal prospective in presence of microorganisms due to off centered disk. The bioconvection communication of micropolar nanofluid with slip utilization was determined by Khan et al. [24].

The essential applications of non-Newtonian materials in various era of science are comprehensively acknowledged. The novel aspects of non-Newtonian fluids are the complicated rheology and distinct features. The non-Newtonian fluids included contributions in many biologically liquids, cosmetics, lubrication applications, medicines, mining industries, processing processes etc. The properties of non-Newtonian fluids are essentially distinct when compare with other fluids. In order to understand the rheological prospective of non-Newtonian materials, scientists have claimed different non-Newtonian models. The Casson nanoliquid is one which use to examine the shear thinning prospective. The fluctuation in shear stress and yield stress results different shape of Casson liquid. The behavior of blood and ink is treated as Casson liquid [25–28].

Following to the dynamic applications of bioconvection of nanofluids, current flow address the Darcy-Forchheimer flow of Casson nanoliquid subject to the bioconvection application and variable thermal features. The summarized objective for performing the analysis is:

- To examine the thermal transport of Casson nanoliquid containing the microorganisms.
- The thermal conductivity of nanofluid is assumed to be variable nature to access the more enhanced transportation pattern.
- The Cattaneo–Christov theory relations are followed to modify the heat and concentration equations.
- The radiation phenomenon is taken into account and impact of Prandtl number and radiation parameter are addressed in terms of effective Prandtl approach.
- A 3-D graphical analysis is performed for velocity, nanofluid temperature, concentration and microorganisms profile.

2. Mathematical modeling

A 2-D and unsteady flow pattern of Casson nanoliquid is assumed. The accelerated stretched surface induced the flow with sinusoidal type velocity. The Casson nanoliquid contains the microorganisms. The thermal features of non-Newtonian (Casson) model are assessed by using the variable thermal conductivity relations. The porous space mechanism is inspected by using the Darcy-Forchheimer law. The activation energy enrollment is defined in the concentration equation. The magnetic force is normally imposed to the direction of flow pattern. The improved relations namely Cattaneo–Christov modifications are used in the concentration and energy equations. The nanofluid temperature is defined with T, concentration with C while microorganism is symbolized with N. The velocity components along the surface and normal to the surface are defined by u and v, respectively. The problem is modeled in terms of following equations:

$$\frac{\partial u}{\partial x}+\frac{\partial v}{\partial y}=0, \tag{1}$$

$$\frac{\partial u}{\partial t}+u\frac{\partial u}{\partial x}+v\frac{\partial u}{\partial y}=\nu\left(1+\frac{1}{A}\right)\frac{\partial^2 u}{\partial y^2}+\frac{g}{\rho_f}\begin{bmatrix}\rho_f(1-c_\infty)(T-T_\infty)\beta^*\\-(\rho_p-\rho_f)(c-c_\infty)\\-(n-n_\infty)\gamma(\rho_m-\rho_f)\end{bmatrix}-\frac{\sigma_M B^2 u}{\rho_f}-\frac{\nu}{k_p}u-Gu^2, \tag{2}$$

$$\frac{\partial T}{\partial t}+u\frac{\partial T}{\partial x}+v\frac{\partial T}{\partial y}+\Upsilon_T\begin{bmatrix}\frac{\partial^2 T}{\partial t^2}+2u\frac{\partial^2 T}{\partial x\partial t}+2v\frac{\partial^2 T}{\partial y\partial t}\\+\frac{\partial v}{\partial t}\frac{\partial T}{\partial y}+u\frac{\partial u}{\partial x}\frac{\partial T}{\partial x}+v\frac{\partial v}{\partial y}\frac{\partial T}{\partial y}\\+u\frac{\partial v}{\partial x}\frac{\partial T}{\partial y}+v\frac{\partial u}{\partial y}\frac{\partial T}{\partial x}\\+2uv\frac{\partial^2 T}{\partial x\partial y}+u^2\frac{\partial^2 T}{\partial x^2}+v^2\frac{\partial^2 T}{\partial y^2}\end{bmatrix}=\frac{1}{(\rho c)_f}\frac{\partial}{\partial y}K(T)\left(\frac{\partial T}{\partial y}\right)+\frac{16T_\infty^3\sigma_r}{3(\rho c)_f k_r}\frac{\partial^2 T}{\partial y^2}$$
$$+\Lambda_\tau\left\{D_B\frac{\partial T}{\partial y}\frac{\partial C}{\partial y}+\frac{D_T}{T_\infty}\left(\frac{\partial T}{\partial y}\right)^2\right\}, \tag{3}$$

$$\frac{\partial C}{\partial t}+u\frac{\partial C}{\partial x}+v\frac{\partial C}{\partial y}+\Upsilon_C\begin{bmatrix}\frac{\partial^2 C}{\partial t^2}+2u\frac{\partial^2 C}{\partial x\partial t}+2v\frac{\partial^2 C}{\partial y\partial t}\\+\frac{\partial v}{\partial t}\frac{\partial C}{\partial y}+u\frac{\partial u}{\partial x}\frac{\partial C}{\partial x}+v\frac{\partial v}{\partial y}\frac{\partial C}{\partial y}\\+u\frac{\partial v}{\partial x}\frac{\partial C}{\partial y}+v\frac{\partial u}{\partial y}\frac{\partial C}{\partial x}\\+2uv\frac{\partial^2 C}{\partial x\partial y}+u^2\frac{\partial^2 C}{\partial x^2}+v^2\frac{\partial^2 C}{\partial y^2}\end{bmatrix}=D_B\frac{\partial^2 C}{\partial y^2}+\frac{D_T}{T_\infty}\frac{\partial^2 T}{\partial y^2}$$
$$-kr^2(C-C_\infty)\left(\frac{T}{T_\infty}\right)^2\exp\left(\frac{-E_a}{\kappa T}\right), \tag{4}$$

$$\frac{\partial N}{\partial t}+u\frac{\partial N}{\partial x}+v\frac{\partial N}{\partial y}=D_m\left(\frac{\partial^2 N}{\partial y^2}\right)-\frac{b_n w_n}{(C_w-C_\infty)}\left[\frac{\partial}{\partial y}\left(N\frac{\partial C}{\partial y}\right)\right], \tag{5}$$

with time t , Casson fluid parameter A, fluid density ρ_f, gravity g, kinematic viscosity ν, nanoparticles density ρ_p, motile density ρ_m, electrical conductivity σ, volume expansion coefficient β^*, magnetic field strength B, Forchheimer coefficient $G=C_F/x\sqrt{k_p}$, permeability parameter k_p, thermal diffusivity α_c, heat flux relaxation time δ_T , Stefan Boltzmann constant σ_r, Boltzmann constant k_r, effective heat fluid capacity to base liquid heat capacity ratio $\Lambda_\tau=(\rho c)_p/(\rho c)_f$, thermal flux relaxation time T_C, swimming cells speed w_n, diffusion constant D_B, thermophoretic diffusion D_T, mass flux relaxation time Υ_C , reaction rate k_r, rate constant n, activation energy E_a, chemotaxis constant b_n and microorganisms diffusion constant D_m.

The thermal conductivity associated with equation (3) is assumed as variable nature with following expressions:

$$K(T)=K_\infty\left(1+\varepsilon\frac{T-T_\infty}{\Delta T}\right), \tag{6}$$

with thermal dependence conductivity ε and ambient liquid conductivity K_∞.

For accelerated flow, the boundary conditions are:

$$u=u_\omega=bx\sin\omega t,\quad v=0,\quad T=T_w,\quad C=C_w, N=N_w \text{ at }\quad y=0,\quad t>0, \tag{7}$$

$$u\to 0,\quad T\to T_\infty,\ C\to C_\infty, N\to N_\infty\quad \text{at}\quad y\to\infty. \tag{8}$$

Following variable are introduced to formulate the governing equations into dimensionless forms:

$$\eta=\sqrt{\frac{b}{\nu}}y,\quad \tau=t\omega,\ u=bxf_y(\eta,\tau),\quad v=-\sqrt{\nu b}f(\eta,\tau), \tag{9}$$

$$\theta(\eta,\tau)=\frac{T-T_\infty}{T_w-T_\infty}, \varphi(\eta,\tau)=\frac{C-C_\infty}{C_w-C_\infty}, \chi(\eta,\tau)=\frac{N-N_\infty}{N_w-N_\infty}, \tag{10}$$

$$\left(1+\frac{1}{A}\right)f_{\eta\eta\eta}+ff_{yy}-Sf_{y\tau}-(1+G_r)f_y^2-Mf_y+\lambda(\theta-Nr\varphi-Rb\chi)=0, \tag{11}$$

$$\left(\frac{1+Rd}{\Pr}\right)\left[(1+\varepsilon\theta)\theta_{yy}+\varepsilon\left(\theta_y\right)^2\right]+\left(f\theta_y-S\varphi_\tau+Nt\left(\theta_y\right)^2+Nb\theta_y\varphi_y\right)-\delta_T\begin{pmatrix}S^2\theta_{\tau\tau}+ff_y\theta_y\\+f^2\theta_{yy}-2Sf\theta_{y\tau}\\-Sf_\tau\theta_y\end{pmatrix}=0, \tag{12}$$

$$\varphi_{yy}+Scf\varphi_y+\frac{Nt}{Nb}\theta_{\eta\eta}-(Sc)S\varphi_\tau-(Sc)\delta_c\left(S^2\varphi_{\tau\tau}+ff_y\varphi_y+f^2\varphi_{yy}-2Sf\varphi_{y\tau}-Sf_\tau\varphi_y\right)=0, \tag{13}$$

$$\chi_{\eta\eta}-S(Lb)\chi_\tau+Lb\chi_\eta-Pe[\varphi_{\eta\eta}(\chi+\varpi)+\chi_\eta\varphi_\eta]=0, \tag{14}$$

with boundary conditions:

$$f_\eta(0,\tau)=\sin\tau,\ f(0,\tau)=0,\theta(0,\tau)=1,\varphi(0,\tau)=1,\chi(0,\tau)=1, \tag{15}$$

$$f_\eta(\infty,\ \tau)\to 0,\ \theta(\infty,\ \tau)\to 0,\varphi(\infty,\ \tau)\to 0,\chi(\infty,\ \tau)\to 0, \tag{16}$$

with $S=\omega/b$ (ooscillating frequency to stretching rate ratio), $Ha=\sqrt{\sigma_M B_0^2/\rho_f b}$, (Hartmann number), $\lambda=\beta^* g(1-C_\infty)(T_w-T_\infty)/\ b^2x$ (mixed convection parameter), $Nr=(\rho_p-\rho_f)(C_w-C_\infty)/\beta^*\rho_f(1-C_\infty)T_\infty$ (bbuoyancy ratio constant), $Gr=C_F/\sqrt{k_p}$ (inertia coefficient) $Rb=\gamma^*(N_w-N_\infty)(\rho_m-\rho_f)/\beta^*\rho_f(1-C_\infty)(T_w-T_\infty)$ (bioconvection Rayleigh number), $Nb=\Lambda_t D_B(C_w-C_\infty)/\nu$ (Brownian motion parameter), $\varpi=N_\infty/(N_w-N_\infty)$ (microorganisms concentration difference), $N_r=16\sigma_r T_\infty^3/3k_r k$ (radiation parameter), $Lb=\nu/\ D_m$ (bioconvection Lewis number), $E=\frac{E^*}{kT_\infty}$, (activation energy constant), $Pe=b_1 w_c/D_m$ (Peclet number), $Nt=\Lambda_\tau D_T(T_w-T_\infty)/\ T_\infty\nu$ (thermophoresis parameter), $\delta_T=\Upsilon_T b$ is thermal relaxation parameter, $Sc=\nu/D_B$ (Schmidt number) and $\delta_C=\Upsilon_C b$ (concentration relaxation parameter).

Eq. (12) is further modified in terms of effective Prandtl number

$$\frac{1}{\Pr_{eff}}\left[(1+\varepsilon\theta)\theta_{yy}+\varepsilon\left(\theta_y\right)^2\right]+\left(f\theta_y-S\varphi_\tau+Nt\left(\theta_y\right)^2+Nb\theta_y\varphi_y\right)-\delta_T\begin{pmatrix}S^2\theta_{\tau\tau}+ff_y\theta_y\\+f^2\theta_{yy}-2Sf\theta_{y\tau}\\-Sf_\tau\theta_y\end{pmatrix}=0, \tag{17}$$

with $\Pr_{eff}=(1+Rd)/\Pr$.

For Casson liquid, wall shear force is:

$$C_f=\frac{\tau_w}{\rho_f u_w^2}=\frac{\left(\tau_{xy}\right)_{\bar{y}=0}}{\rho_f u_w^2},\ \mathrm{Re}_x^{1/2}C_f=\left(1+\frac{1}{A}\right)f_{yy}(0,\tau). \tag{18}$$

Moreover local Nusselt number Nu_x, Sherwood number Sh_x, motile density number Nn_x are defined as:

$$Nu_x\mathrm{Re}_x^{-1/2}=-\left(1+\frac{4}{3}Rd\right)\theta_\eta(0,\tau),\frac{Su}{\sqrt{\mathrm{Re}_x}}=-\varphi_\eta(0,\tau),\frac{Nn_x}{\sqrt{\mathrm{Re}_x}}=-\chi_\eta(0,\tau). \tag{19}$$

3. Analytical solution

In this section, homotopy analysis scheme is introduced to discuss the solution procedure. With efficient accuracy, this scheme is employed by many researchers [29–34]. Following initial approximations are considered to start the analytical procedure:

$$\left.\begin{array}{l}f_0(\eta,\tau)=\sin\tau-e^{-\eta}\sin\tau,\ \theta_0(\eta)=e^{-\eta},\\ \varphi_0(\eta)=e^{-\eta},\chi_0(\eta)=e^{-\eta}.\end{array}\right\} \tag{20}$$

Following relations are satisfied against above initial approximations.

$$\pounds_f[\pi_1+\pi_2 e^{y}+\pi_3 e^{-y}]=0, \tag{21}$$

$$\pounds_\theta[\pi_4 e^{y}+\pi_5 e^{-y}]=0, \tag{22}$$

$$\pounds_\varphi[\pi_6 e^{y}+\pi_7 e^{-y}]=0, \tag{23}$$

$$\pounds_\chi[\pi_8 e^{y}+\pi_9 e^{-y}]=0, \tag{24}$$

where $\pi_i(i=1,\ 2,\ldots,9)$ symbolize the arbitrary constants.

4. Convergence analysis

In homotopic algorithm, the assessment of convergence mechanism is quite compulsory for validation of numerical data. This task is completed with examining the numerical values of auxiliary parameters $h_f, h_\theta\ h_\varphi$ and h_χ. Fig. 1 (h-curve) is proceeded to inspect the

range of such parameters. For excellent numerical accuracy the range of such parameters is $-1.3 \leq h_f \leq -0.1$, $-0.6 \leq h_\theta \leq -0.2$, $-1.1 \leq h_\varphi \leq 0$ and $-1 \leq h_\chi \leq 0$. The validation task for solution is completed by comparing the numerical data with analysis of Turkyilmazoglu [34] in Table 1 which reflects a good agreement between both investigations.

5. Physical explanation of results

After the successful computations of problem via analytical scheme, this section highlights the physical interference of results when different flow parameters get numerical fixed values.

5.1. Velocity profile

Fig. 2(a–c) examined the change in velocity f_n against time τ for inertia coefficient G_r, Casson liquid constant A and mixed convection parameter λ. Fig. 2(a) predicts that a decreasing change in f_n against τ is observed when inertia coefficient constant get maximum variation. An oscillatory nature of velocity is resulted with decreasing magnitude. The interaction of strong inertial forces produces a decrement in the velocity. Fig. 2(b) reports the behavior of f_n with enrollment of Casson liquid constant A. Again, when Casson liquid parameter assigns leading numerical variation, the velocity profile get slower. The physical insight of mixed convection parameter λ on f_n is visualized graphically in Fig. 2(c). An arising oscillatory profile of velocity is reported with λ.

5.2. Temperature profile

Fig. 3(a–d) is prepared in order to check the influence of inertia coefficient G_r and Casson liquid constant A, thermal relaxation constant δ_T , effective Prandtl number Pr_{eff}, buoyancy constantNr , variable thermal conductivity parameter ε, thermophoresis constant Nt and Brownian constant Nb on nanofluid temperature θ. All the graphical simulations are presented at $\tau = \pi/2$. Fig. 3(a) fluctuates the profile of θ for G_r and A. The progressive nanofluid temperature against higher G_r and A is observed from this curve. The enhancement in θ due to G_r is physically defended due to interaction of inertial forces. Fig. 3(b) pronounced the contribution of effective Prandtl number Pr_{eff} and thermal relaxation constant δ_T on θ. A turning down temperature of nanoliquid is visualized for Pr_{eff} and δ_T. The effective Prandtl number contains the combined feature of Prandtl number and radiation constant. A direct relation of Pr_{eff} is formulated with Prandtl number. Physically, the thermal diffusivity is minimum for higher Prandtl constant which reduce the temperature. Moreover, the nanofluid temperature also shows a slower profile for δ_T. The results claimed via Fig. 3(c) reflect that an enhancement in θ is measured for buoyancy constant Nr and variable thermal conductivity parameter ε . The physical mechanism for enhancement in θ with Nr is attributed due to presence of buoyancy forces. The consideration of variable thermal conductivity is more effective to improve the fluctuation in nanofluid temperature. The graphical illustration for the contribution of thermophoresis constant Nt and Brownian constant Nb in profile of θ is depicted in Fig. 3(d). The thermophoresis and Brownian parameters are two major factors in Buongiorno nanofluid model. A an increasing nanofluid temperature is pointed out for both constants. The thermophoresis pattern in yield out due to the famous thermophoresis phenomenon which consists of departure nanofluid particles from heated zone to the cooler area. Similarly, the Brownian constants enhanced the temperature as it replicates the random fluid movement in the heated frame.

5.3. Concentration profile

Fig. 4(a–d) aims to examine the change in nanofluid concentration φ for G_r , A , Nt , Nb , δ_C , Sc , E and Nr. From Fig. 4(a), a rise in φ is signified with G_r and A . The role of thermophoretic constant Nt and Brownian constant Nb on φ is worked out in Fig. 4(b). Here, an increasing and declining change in φ is observed for Nt and Nb, respectively. The increment φ due to Nt is noticed while reverse change in φ is noted when Nb is maximum. Fig. 4(c) gives the physical prospective of concentration relaxation δ_C and Schmidt number Sc on φ.

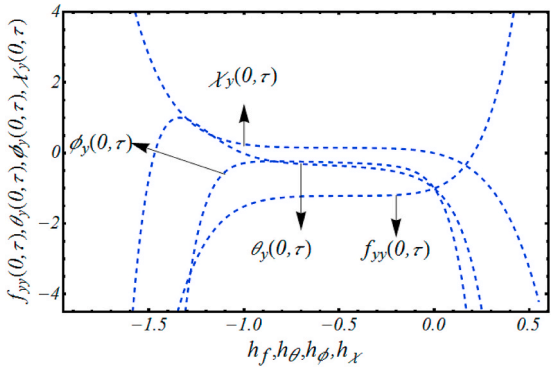

Fig. 1. h-curve for all profiles.

Table 1
Solution validation as for $f''(0,\tau)$ when $A \to \infty, S = \lambda = Gr = Nr = Rb = 0.$ and $\tau = \pi/2$.

M	Turkyilmazoglu [34]	Present results
0	−1.000000	−1.000000
0.5	−1.224744	−1.224743
1	−1.414213	−1.414211
1.5	−1.581138	−1.581138

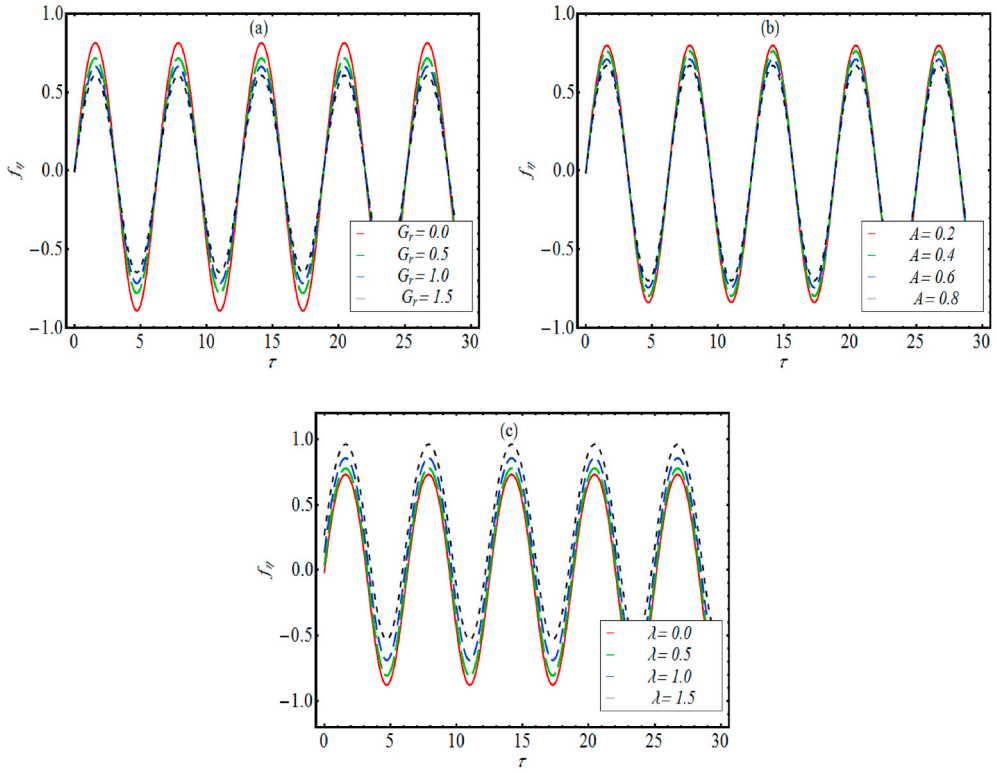

Fig. 2. (a–c): Change in f_n for (a) G_r, (b) A (c) λ.

When leading numerical values are given to both constant, the concentration turn downs slightly. Physical aspects behind decrement in φ is due *Sc* is due to reverse relation of Schmidt constant with mass diffusivity. The results incorporated via Fig. 4(d) claimed that nanofluid concentration profile is rapidly change with increasing manner due to *E* and *Nr*. The activation energy parameter contributes effectively to improve the reaction pattern in many physical and chemical procedures.

5.4. Microorganisms profile

In order to check out the role of inertial constant G_r , Casson liquid constant A , bioconvection Lewis number *Lb* and Peclet number*Pe* on microorganisms profile χ, Fig. 5(a and b) is sketched. Fig. 5(a) shows that, with maximum change in G_r and A, the microorganisms profile boost up more progressively. The presence of non-Newtonian material and Darcy porous space help to improve the microorganisms profile. Fig. 5(b) reports a decreasing behavior of χ with increasing values assign to *Lb* and *Pe*. The Peclet number ensured a reverse relationship with motile density which is responsible to such depressing behavior of. χ.

5.5. -D illustration of velocity, temperature, concentration and microorganisms profile

In current time dependent flow, the accelerated flow is induced with periodically moving surface. The 3-D illustration of velocity f_η with η and time τ, is presented in Fig. 6 when the flow parameters kept fixed. An accelerating behavior of f_η is observed with very minor phase shift. A gradual variation in f_η is seen along y-axis without oscillation. Fig. 7 addressed the 3-D nature of temperature θ . A linear change in θ is observed without any oscillating behavior. The 3-D profile and concentration φ and microorganism χ is observed in Figs. 8 and 9, respectively. No oscillation in both profiles are predicted again.

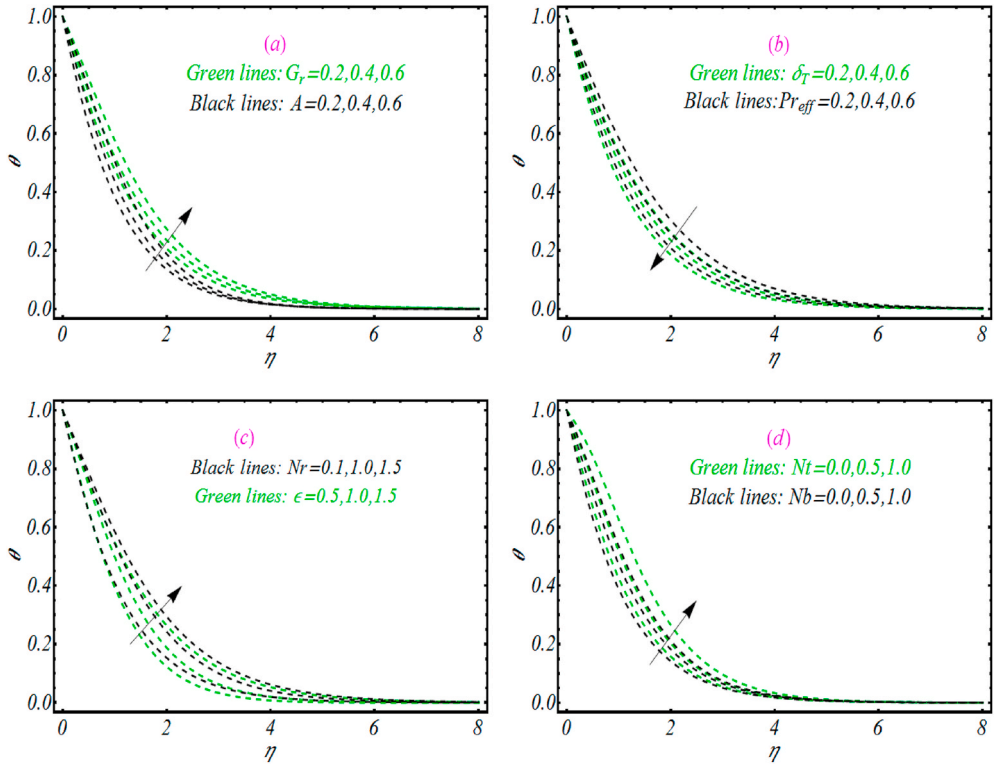

Fig. 3. (a–d): Change in θ for (a) G_r and A (b) δ_T and Pr_{eff}(c) Nr and ε (c) Nt and Nb.

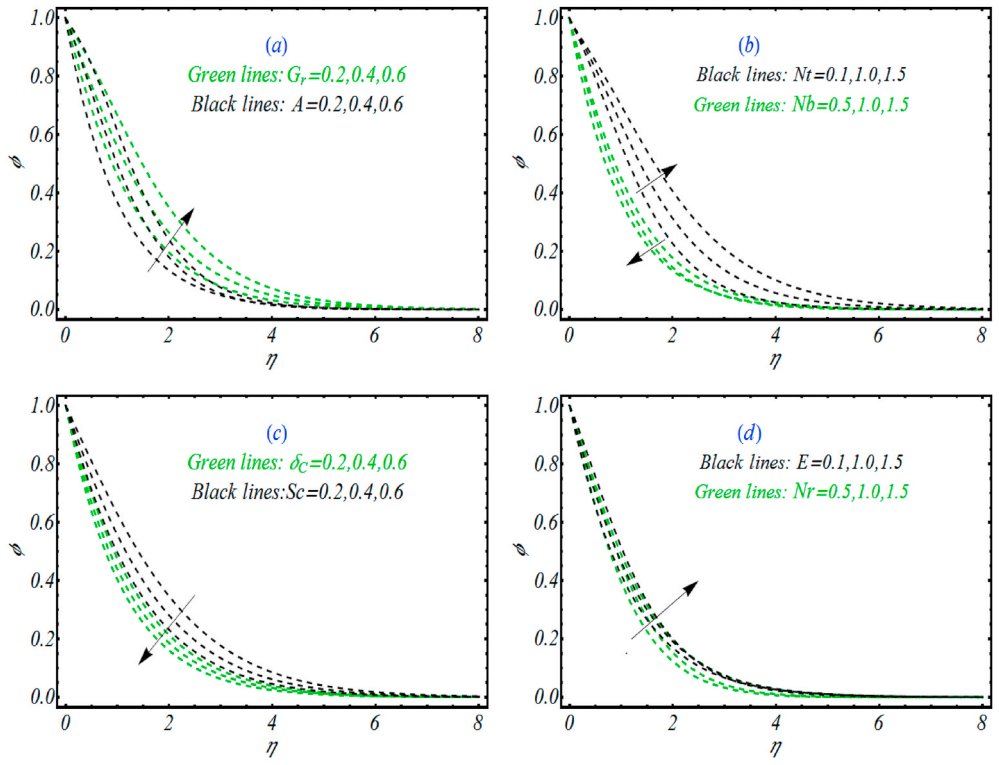

Fig. 4. (a–d): Change in φ for (a) G_r and A (b) Nt and Nb. (c) δ_C and Sc (c) E and Nr

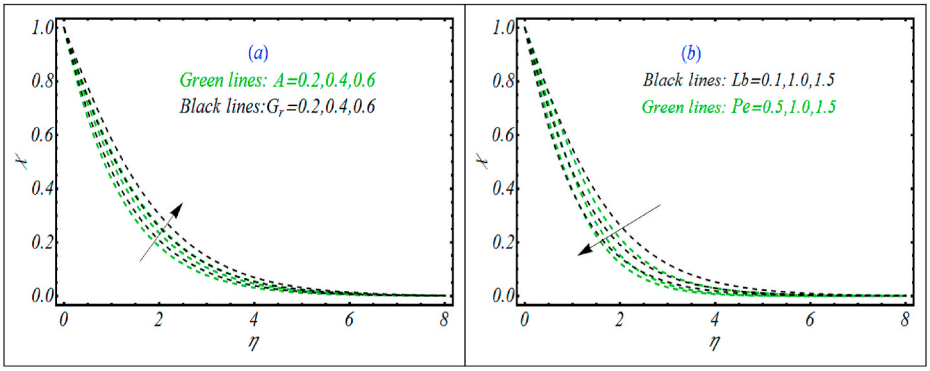

Fig. 5. (a–b): Change in χ for (a) G_r and A (b) Lb and Pe.

5.6. Physical quantities

The numerical values are calculated Gr, Nr, Rb, A, M, λ and Pr_{eff} by against relation of $-\theta_\eta(0,\tau)$, $-\varphi_\eta(0,\tau)$ and $-\chi_\eta(0,\tau)$ in Table 2. The increasing change $-\theta_\eta(0,\tau)$, $-\varphi_\eta(0,\tau)$ and $-\chi_\eta(0,\tau)$ against flow parameters like λ and Pr_{eff} is noted while all other parameters slow down the heat, mass and motile transportation rate.

6. Conclusions

The applications of bioconvection for the thermal transport of Casson nanoliquid is inspected in this analysis. The significances of Darcy-Forchheimer relation, invariable thermal conductivity futures and activation energy are also addressed with fundamental laws. The problem is formulated in terms of PDE's which are analytically solved. A comprehensive graphical analysis and 3-D illustration of problem is presented. The prime findings from current analysis are:

- ➢ The applications of inertial coefficient and Casson liquid constant slow down the velocity.
- ➢ The transportation of heat transfer pattern is effectively improved by considering the variable thermal relations.
- ➢ The nanofluid temperature gets raised for inertial coefficient, Cason liquid parameter and thermophoresis constant.
- ➢ The nanofluid concentration and temperature get slower for concentration relaxation and thermal relaxation constant, respectively.
- ➢ The microorganisms get increasing change for Casson liquid constant and inertial coefficient while slow down for bioconvection Lewis number.
- ➢ A 3-D illustration of temperature, concentration and microorganisms profiles is not of periodic nature.
- ➢ These results convey applications in improvement of thermal energy, solar systems, energy devices, controlling the cooling of devices, petroleum recovery, biofuels etc.

Declaration of competing interest

The authors declare that they have no known competing financial interests or personal relationships that could have appeared to influence the work reported in this paper.

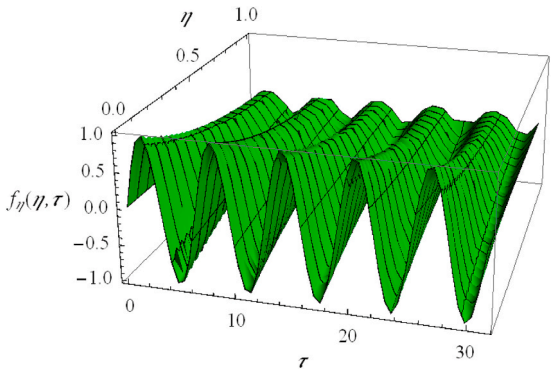

Fig. 6. A 3-D illustration for velocity f_η

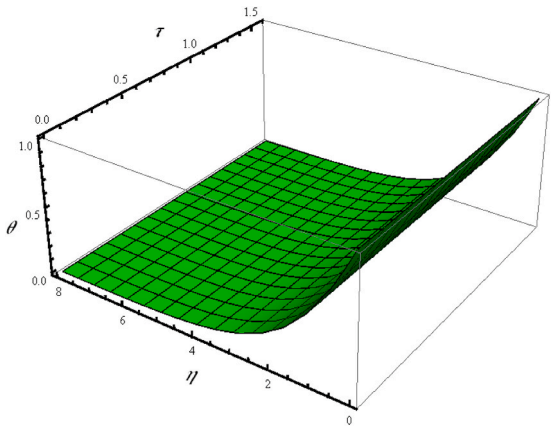

Fig. 7. A 3-D illustration for temperature θ.

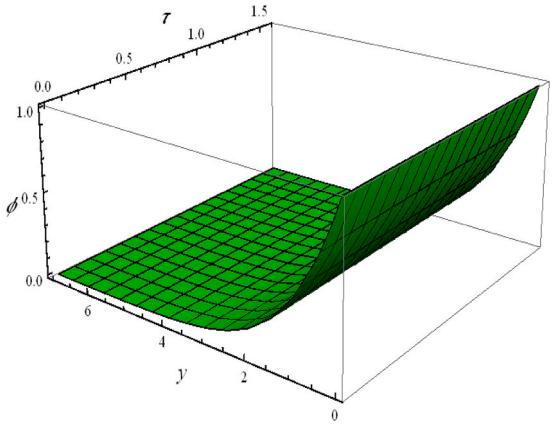

Fig. 8. A 3-D illustration for concentration φ.

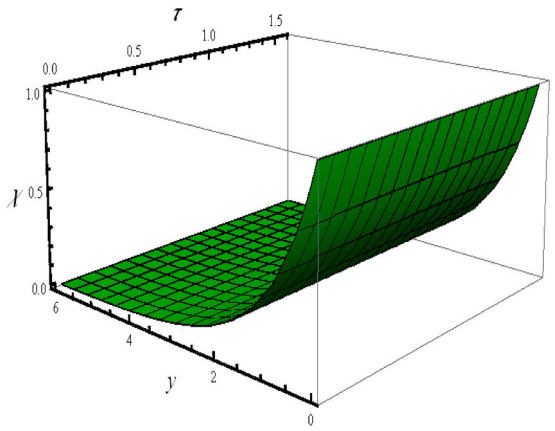

Fig. 9. A 3-D illustration for microorganism.χ.

Table 2
Illustration of $-\theta_\eta(0,\tau)$, $-\varphi_\eta(0,\tau)$ and $-\chi_\eta(0,\tau)$ for different flow parameters.

Gr	*Nr*	*Rb*	*A*	*M*	λ	Pr_{eff}	$-\theta_\eta(0,\tau)$	$-\varphi_\eta(0,\tau)$	$-\chi_\eta(0,\tau)$
0.2	0.3	0.1	0.3	0.5	0.5	0.2	0.42547	0.44345	0.48462
0.6							0.40687	0.41327	0.45053
0.8							0.37466	0.39768	0.43654
0.1	0.4						0.462552	0.4664	0.51626
	0.8						0.437532	0.44978	0.48460
	1.2						0.424546	0.40768	0.44543
		0.2					0.484345	0.49458	0.51431
		0.6					0.456546	0.45898	0.48032
		1.0					0.424976	0.42624	0.47614
			0.2				0.48205	0.49343	0.536543
			0.4				0.45256	0.45564	0.52042
			0.6				0.41664	0.42087	0.50554
				0.2			0.43654	0.46128	0.52566
				0.4			0.38646	0.416589	0.477567
				0.8			0.348652	0.36321	0.43234
					0.2		0.43646	0.45346	0.51564
					0.4		0.445465	0.51555	0.54564
					0.6		0.47035	0.552678	0.57523
						0.4	0.52354	0.441678	0.50552
						0.8	0.54546	0.496678	0.53535
						14	0.60868	0.53281	0.57575

Acknowledgment

The authors extend their appreciation to the Deanship of Scientific Research at King Khalid University, Abha 61413, Saudi Arabia for funding this work through research groups program under Grant No. R.G.P-1/96/42.

References

[1] S.U.S. Choi, Enhancing thermal conductivity of fluids with nanoparticles, ASME-Publications-Fed 231 (1995) 99–106.
[2] J. Buonigiorno, Convective transport in nanofluids, J. Heat Tran. 128 (2010) 240–250.
[3] A. Hamid Hashim, M. Khan, Thermo-physical characteristics during the flow and heat transfer analysis of GO-nanoparticles adjacent to a continuously moving thin needle, Chin. J. Phys. 64 (2020) 227–240.
[4] M. Turkyilmazoglu, Single phase nanofluids in fluid mechanics and their hydrodynamic linear stability analysis, Comput. Methods Progr. Biomed. 187 (2020), 105171.
[5] M.I. Khan, A. Kumar, T. Hayat, M. Waqas, R. SIngh, Entropy generation in flow of Carreau nanofluid, J. Mol. Liq. 278 (2019) 677–687.
[6] A. Hajizadeh, N.A. Shah, S.I.A. Shah, I.L. Animasaun, M. Rahimi-Gorji, I.M. Alarifi, Free convection flow of nanofluids between two vertical plates with damped thermal flux, J. Mol. Liq. 289 (2019), 110964.
[7] S.U. Khan, S.A. Shehzad, A. Rauf, Z. Abbas, Thermally developed unsteady viscoelastic micropolar nanofluid with modified heat/mass fluxes: a generalized model, Physica A: statistical Mechanics and its Applications, Physica A 550 (2020), 123986.
[8] A. Majeed, A. Zeeshan, M.M. Bhatti, R. Ellahi, Heat transfer in magnetite (Fe_3O_4) nanoparticles suspended in conventional fluids: refrigerant-134a ($C_2H_2F_4$), kerosene ($C_{10}H_{22}$), and water (H_2o) under the impact of dipole, Heat Tran. Res. 51 (3) (2020) 217–232.
[9] M.U. Ashraf, M. Qasim, A. Wakif, M.I. Afridi, I.L. Animasaun, A Generalized Differential Quadrature Algorithm for Simulating Magnetohydrodynamic Peristaltic Flow of Blood-based Nanofluid Containing Magnetite Nanoparticles: A Physiological Application, Numerical Methods for Partial Differential Equations, 2020, https://doi.org/10.1002/num.22676.
[10] M.I. Khan, F. Alzahrani, Dynamics of activation energy and nonlinear mixed convection in Darcy-forchheimer radiated flow of Carreau nanofluid near stagnation point region, J. Therm. Sci. Eng. Appl. 13 (5) (2021), 051009.
[11] M.M. Bhatti, C.M. Khalique, T.A. Bég, O.A. Bég, A. Kadir, Numerical study of slip and radiative effects on magnetic Fe 3 O 4-water-based nanofluid flow from a nonlinear stretching sheet in porous media with Soret and Dufour diffusion, Mod. Phys. Lett. B 34 (2) (2020), 2050026.
[12] Z. Nisar, T. Hayat, A. Alsaedi, B. Ahmad, Significance of activation energy in radiative peristaltic transport of Eyring-Powell nanofluid, Int. Commun. Heat Mass Tran. 116 (2020), 104655.
[13] M.M. Bhatti, Biologically inspired intra-uterine nanofluid flow under the suspension of magnetized gold (Au) nanoparticles: applications in nanomedicine, Inventions 6 (2) (2021) 28.
[14] R.E. Abo-Elkhair, M.M. Bhatti, Kh.S. Mekheimer, Magnetic force effects on peristaltic transport of hybrid bio-nanofluid (Au-Cu nanoparticles) with moderate Reynolds number: an expanding horizon, Int. Commun. Heat Mass Tran. 1 (123) (2021), 105228.
[15] A. Shahid, H.L. Huang, C.M. Khalique, M.M. Bhatti, Numerical analysis of activation energy on MHD nanofluid flow with exponential temperature-dependent viscosity past a porous plate, J. Therm. Anal. Calorim. 143 (3) (2021) 2585–2596.
[16] M.M. Bhatti, Marin Marin, Zeeshan Ahmed, R. Ellahi, Sara I. Abdelsalam, Swimming of motile gyrotactic microorganisms and nanoparticles in blood flow through anisotropically tapered arteries, Frontiers in Physics 8 (2020) 95. Apr 8.
[17] A.V. Kuznetsov, The onset of nanofluid bioconvection in a suspension containing both nanoparticles and gyrotactic microorganisms, Int. Commun. Heat Mass Tran. 37 (10) (2010) 1421–1425.
[18] A.V. Kuznetsov, Nanofluid bioconvection in water-based suspensions containing nanoparticles and oxytactic microorganisms: oscillatory instability, Nanoscale Res. Lett. 6 (2011) 100.
[19] Md J. Uddin, M.N. Kabir, O.A. Beg, Computational investigation of Stefan blowing and multiple-slip effects on buoyancy-driven bioconvection nanofluid flow with microorganisms, Int. J. Heat Mass Tran. 95 (2016) 116–130.
[20] A.M. Alwatban, S.U. Khan, H. Waqas, I. Tlili, Interaction of Wu's slip features in bioconvection of Eyring Powell nanoparticles with activation energy, Processes 7 (11) (2019) 859.
[21] M.I. Khan, F. Haq, S.A. Khan, T. Hayat, M. Imran Khan, Development of thixotropic nanomaterial in fluid flow with gyrotactic microorganisms, activation energy, mixed convection, Comput. Methods Progr. Biomed. 187 (2020), 105186.

[22] N.S. Khan, Q. Shah, A. Bhaumik, P. Kumam, P. Thounthong, I. Amiri, Entropy generation in bioconvection nanofluid flow between two stretchable rotating disks, Sci. Rep. 10 (2020), 4448.
[23] Y.- Qing Song, S.A. Khan, M. Imran, H. Waqas, S.U. Khan, M. Ijaz Khan, S. Qayyum, Yu-Ming Chu, Applications of modified Darcy law and nonlinear thermal radiation in bioconvection flow of micropolar nanofluid over an off centered rotating disk, Alexandria Engineering Journal 60 (5) (2021) 4607–4618.
[24] M. Ijaz Khan, H. Waqas, S.U. Khan, M. Imran, Yu-Ming Chu, A. Abbasi, S. Kadry, Slip flow of micropolar nanofluid over a porous rotating disk with motile microorganisms, nonlinear thermal radiation and activation energy, Int. Commun. Heat Mass Tran. 122 (2021), 105161.
[25] K.U. Rehman, E.A. Algehyne, F. Shahzad, El-Sayed M. Sherif, Yu-Ming Chu, On thermally corrugated porous enclosure (TCPE) equipped with casson liquid suspension: finite element thermal analysis, Case Studies in Thermal Engineering 25 (2021) 100873.
[26] M.M. Nandeppanavar, S. Vaishali, M.C. Kemparaju, N. Raveendra, Theoretical analysis of thermal characteristics of casson nano fluid flow past an exponential stretching sheet in Darcy porous media, Case Studies in Thermal Engineering 21 (2020), 100717.
[27] M.I. Khan, Transportation of hybrid nanoparticles in forced convective Darcy-Forchheimer flow by a rotating disk, Int. Commun. Heat Mass Tran. 122 (2021), 105177.
[28] M.M. Bhatti, S.U. Khan, O.A. Beg, A. Kadir, Differential transform solution for hall and Ion slip effects on radiative-convective Casson flow from a stretching sheet with convective heating, Heat Tran. Asian Res. *49* (2) (2020) 872–888.
[29] M. Turkyilmazoglu, Analytic approximate solutions of rotating disk boundary layer flow subject to a uniform suction or injection, Int. J. Mech. Sci. 52 (2010) 1735–1744.
[30] M. Turkyilmazoglu, The analytical solution of mixed convection heat transfer and fluid flow of a MHD viscoelastic fluid over a permeable stretching surface, Int. J. Mech. Sci. 77 (2013) 263–268.
[31] M. Turkyilmazoglu, Convergence accelerating in the homotopy analysis method: a new approach, Adv. Appl. Math. Mech. 10 (4) (2018) 925–947.
[32] S.U. Khan, H.M. Ali, Swimming of gyrotactic microorganisms in unsteady flow of eyring powell nanofluid with variable thermal features: some bio-technology applications, Int. J. Thermophys. 41 (2020) 159.
[33] I. Ahmad, S. Aziz, N. Ali, S.U. Khan, Radiative unsteady hydromagnetic 3D flow model for Jeffrey nanofluid configured by an accelerated surface with chemical reaction, Heat Transfer 50 (2021) 942–965.
[34] M. Turkyilmazoglu, The analytical solution of mixed convection heat transfer and fluid flow of a MHD viscoelastic fluid over a permeable stretching surface, Int. J. Mech. Sci. 77 (2013) 263–268.